

Evolution of the parallel and perpendicular ion velocity distribution functions in pulsed helicon plasma sources obtained by time resolved laser induced fluorescence

Costel Biloiu^{1,4}, Xuan Sun¹, Edgar Choueiri², Forrest Doss¹, Earl Scime¹, John Heard³, Rostislav Spektor² and Daniel Ventura¹

¹ Department of Physics, West Virginia University, Morgantown, WV 26506, USA

² Department of Mechanical and Aerospace Engineering, Princeton University, Princeton, NJ 08544, USA

³ Department of Physics, Clarion University of Pennsylvania, Clarion, PA 16214, USA

E-mail: costel.biloiu@mail.wvu.edu

Received 16 July 2005, in final form 5 October 2005

Published 27 October 2005

Online at stacks.iop.org/PSST/14/766

Abstract

The temporal evolution of parallel and perpendicular ion velocity distribution functions (ivdf) in a pulsed, helicon-generated, expanding, argon plasma is presented. The ivdf's temporal evolution during the pulse was determined with time resolved (1 ms resolution), laser induced fluorescence. The parallel ivdf measurements indicate that, in the expansion region of the plasma and for certain operational parameters, two ion populations exist: a population moving at supersonic speeds (1.1 Mach) resulting from acceleration in an electric double layer (EDL) and a slow moving population (0.7 Mach) generated by local ionization. After 100 ms, although present, the EDL is not fully developed and has not reached a steady-state. Measurements of the perpendicular ivdf indicate constant radial expansion, with ion speeds of $\approx 400 \text{ m s}^{-1}$, in the expansion region.

1. Introduction

High plasma densities generated at low pressure (few millitorrs) and for relatively modest input power (200 W–2 kW) make helicon plasma sources suitable for a wide range of applications. For example, it has been shown that uniform fluxes with high plasma density and reduced ion energy near a processing substrate can be obtained [1, 2]. Arrays of compact helicon plasma sources have also been shown to produce uniform plasmas over large areas [3, 4]. For plasma etching, high etching rates ($1.5 \mu\text{m min}^{-1}$) with a minimum anisotropy of 0.97 were obtained with an expanding SF₆ helicon plasma [5]. By pulsing a helicon discharge, even larger plasma densities,

and therefore etching rates, can be obtained since larger input powers can be employed. For thin film deposition, researchers have shown that changing the duty cycle of a pulsed helicon discharge may reduce the internal stress induced in the deposited silicon dioxide films without altering the main properties of the deposited layers. A decrease of the compressive stress with a time constant of 80 μs has been obtained by using pulses of 500 μs with 30–100% duty cycle [6]. A high ionization degree of 65% and a gas temperature of 1000 K have been obtained near the antenna by using a pulsed mode instead of steady-state in an Ar helicon plasma for a pulse 'on' time of 2 ms and input power of 2 kW [7]. Spatial uniformity is expected to improve and the mean ion energy to decrease in the plasma afterglow of a pulsed discharge. Therefore, knowledge of the evolution of the ion velocity distribution function (ivdf) during the pulse

⁴ Author to whom any correspondence should be addressed.

is of critical importance since the width of the ivdf perpendicular to the sample surface (the parallel ion temperature) plays a key role in etching selectivity. The ion velocity parallel to the sample surface, which plays a key role in trench rectangularity, is another important ivdf characteristic to be determined throughout the plasma pulse.

The helicon source as a plasma thruster, as an alternative to chemical propulsion, is a relatively new application of helicon sources. In a thruster application, the ejected plasma flux and the ion flow velocity are the critical source parameters. Promising levels of ion production by a helicon source and subsequent ion heating by an ion cyclotron cell have been observed in the Variable Specific Impulse Magnetoplasma Rocket (VASIMR) which is a plasma thruster concept that relies on rf plasma heating and plasma acceleration in a magnetic nozzle [8, 9]. Another promising application of helicon sources to propulsion relies on energizing the ions exiting the sources through a non-resonant nonlinear ion acceleration mechanism that involves beating electrostatic waves [10]. More recently, three different helicon source experiments have shown that at the open end of a helicon source connected to a larger expansion chamber, an electric double layer (EDL) can spontaneously form [11–14]. Since the EDL accelerates and then ejects ions at supersonic speeds, this phenomenon could provide a simple means of turning a helicon source into a plasma thruster. Argon ions exit speeds between 8 and 15 km s⁻¹, i.e. a few times the ion acoustic speed, have been reported [14, 15]. Pulsing the helicon discharge might solve some important thruster application issues such as plasma detachment or turbulent cross-field diffusion (as observed in magnetic nozzles). Studies on the Mini-Magnetic Plasma propulsion (M2P2) prototype for pulse lengths from one millisecond to several seconds showed an increase in plasma density for a pulse length of 1 ms [16]. The High Power Helicon (HPH) experiment reported plasma densities of $\approx 10^{14}$ cm⁻³ for 10 kW input power and a 200 μ s pulse length [17]. Therefore, for thruster applications, an understanding of the evolution of the ivdf is needed to choose the optimal operational parameters (duty cycle, pulse length, input power, driving frequency) to obtain the desired specific impulse along the expansion direction while minimizing the ion energy in perpendicular direction.

Non-perturbative, spatially resolved measurements of ion velocity distributions can be obtained in argon plasmas by laser induced fluorescence (LIF). Since its first application to plasma diagnosis three decades ago by Stern and Johnson [18], both the technology employed for LIF measurements and the methods used to analyse LIF data are constantly improving [19–22], e.g. tomographic inversions are now routinely used to obtain two-dimensional velocity space measurements at a single spatial location [23–25], and the LIF is applied to many types of plasma discharges and for a wide range of experimental conditions [26]. The magnitudes and directions of ambient electric and even weak magnetic fields in plasmas can also be determined from their effects on the energy levels of the specific quantum states (probed with LIF) of the target particle [27, 28]. Since the probing laser linewidth (typically ≈ 1 MHz in the case of diode lasers and ≈ 10 MHz in the case of dye lasers) is much smaller than the particle absorption linewidth (≈ 1 GHz for particles of $m = 40$ amu at

room temperature and larger for higher temperatures), high resolution measurements of bulk velocity and temperature can be obtained. For a wide range of plasma conditions Doppler broadening dominates over other line broadening mechanisms, e.g. Zeeman splitting, Stark broadening and power broadening. Even in strongly magnetized discharges, for which Zeeman splitting cannot be ignored, the choice of a particular polarization of the pumping laser often reduces the complexity of the measured absorption linewidth to a manageable level while also providing a direct measure of the ambient magnetic field strength. The spatial resolution of LIF measurements, determined by the intersection of the probing laser beam and the fluorescence collection volume, is typically on the order of a few cubic millimetres.

In this work, we investigate the temporal evolution of the parallel and perpendicular ivdf in argon plasma in two pulsed helicon sources. The ivdf's temporal evolution during the pulse has been obtained by using a time and velocity resolved LIF method. The only modification to the experimental apparatus that we typically use for LIF measurements in steady-state plasmas is the addition of a digital oscilloscope on which the LIF emission versus time is averaged over many tens of pulses [29]. A time resolution of 1 ms is sufficient to investigate ion heating by pulsed electrostatic ion-cyclotron beat-waves [10, 30, 31], in helicon sources and the formation of ion beams in pulsed expanding helicon source plasmas [32]. We note that other researchers have used similar techniques to investigate externally imposed, repetitive, transient phenomena in a steady-state background plasma, e.g. the interaction between ions and ion cyclotron waves in argon plasmas [33]. However, those experiments only examined the time-averaged interaction of the ions with the waves.

2. Helicon plasma sources

The descriptions of helicon plasma sources used for investigations in the present experiments are presented in detail elsewhere (see for example [14] for the West Virginia University helicon plasma source and [30] for the Princeton University's Electric Propulsion and Plasma Dynamics Laboratory helicon source). Briefly, the characteristics of these machines are as follows.

2.1. West Virginia University helicon plasma source

The HELIX (Hot hELIcon eXperiment) machine consists of a 61 cm long, 10 cm diameter Pyrex tube mated coaxially with a 91 cm long, 15 cm diameter stainless steel tube. Ten electromagnets produce a magnetic field of 0–1.2 kG along the tube axis. A 19 cm long, half wave, $m = +1$, helical antenna couples the rf energy into the plasma. An rf power source furnishes up to 2 kW over a frequency range of 6–18 MHz. Switching between continuous wave mode and pulse mode as well as changing the pulse duty cycle is accomplished by a pulse generator which modulates the rf source. The plasma produced in the source expands into a 4 m long, 2 m in diameter aluminium diffusion chamber, LEIA (Large Experiment on Instabilities and Anisotropies). The LEIA expansion chamber is surrounded by seven electromagnets which provide an axial magnetic field of 0–300 G. Therefore, under typical operating

conditions, in the connection region between the helicon source and the expansion chamber there exists an axial magnetic field gradient of nearly 1000 G m^{-1} over a distance of about 0.7 m. The HELIX–LEIA system is pumped differentially and the gas inlet valve is near the rf antennae. Thus, there is a slight pressure gradient along the source axis while in the expansion region the pressure is constant, almost one order of magnitude smaller than the source pressure. Under typical working conditions, in the steady-state mode, for argon gas, electron temperatures and densities in HELIX are $T_e \approx 4\text{--}12 \text{ eV}$ and $n_e \approx 10^{11}\text{--}10^{13} \text{ cm}^{-3}$ while in LEIA $T_e \approx 2\text{--}7 \text{ eV}$ and $n_e \approx 1 \times 10^9\text{--}5 \times 10^{11} \text{ cm}^{-3}$ as measured with rf compensated Langmuir probes [24, 34] and a swept frequency microwave interferometer [35].

2.2. Princeton Plasma Propulsion helicon plasma source

The Beating Wave eXperiment (BWx) machine consists of a small Pyrex cylinder, 6 cm in diameter, 37 cm in length, concentrically connected through an electrically floating aluminium plate to a large Pyrex cylinder 20 cm in diameter and 46 cm in length. At the other end of the small cylinder is a molybdenum plate that is electrically floating to minimize sputtering effects. The large cylinder is terminated with an aluminium plate, also electrically floating. A uniform fill pressure of 1–30 mTorr is maintained by a gas feed at the aluminium endplate of the large cylinder and a 150 L s^{-1} turbopump with a conductance controller backed up by a roughing pump. Five electromagnets provide an axial magnetic field of up to 1 kG. A 13 cm long Boswell saddle antenna wrapped around the small cylinder, 8 cm away from the junction between the chambers, is used to create the plasma. The antenna is made from 6.35 mm copper tubing to allow water cooling and is fed by an ENI 13.56 MHz rf power supply able to furnish up to 1.2 kW forward power through a L-type matching network. The rf power is modulated with a pulse generator with adjustable pulse length and duty cycle. Under typical operating parameters, $P = 500 \text{ W}$, $B = 800 \text{ G}$ and $p = 1 \text{ mTorr}$, in argon gas, the on-axis electron temperature and density in the large cylinder are $T_e \approx 3 \text{ eV}$ and $n_e \approx 10^{13} \text{ cm}^{-3}$, respectively.

3. LIF for pulsed argon plasmas

In a steady-state plasma, a typical LIF measurement is a measurement of the time averaged velocity distribution. Weak LIF emission from a steady-state plasma can be detected in the presence of intense background light by modulating the probing laser beam and employing phase synchronous detection, i.e. using a lock-in amplifier. Pulsed plasmas present the additional challenge of requiring time resolution while still detecting weak LIF emission. The minimum time resolution of a LIF measurement is set by the lifetime of the upper quantum level of the pumped transition, usually on the order of a few nanoseconds. Therefore, all repetitive phenomena with a characteristic time larger than a few nanoseconds could be investigated by LIF. In practice, however, time resolution is limited by the need to collect a sufficient number of LIF emission photons for a reasonable signal to noise; the RC time constants of cables; the signal acquisition time requirements of

the available electronics and the particular plasma conditions. When the properties of the measurement electronics are well known, it is possible to improve the time resolution of LIF measurements by reducing the distorting effects of the electronics by digital signal processing. For example, Jackson *et al* [36] performed argon atom LIF measurements on a pulsed plasma (pulse length 5 ms) probed with a broadband laser modulated at 3 kHz. The plasma emission observed with a photomultiplier tube (PMT) detector was processed by lock-in amplifier referenced to the modulation frequency and set to an integration time constant of 1 ms. The effect of the 1 ms time constant, effectively a low pass filter, on the lock-in signal was reduced by digitally recording the lock-in output as a function of time and then separating the ‘true’ time series from the low-pass filter response of the lock-in with a deconvolution algorithm. Previously [29], we have reported measurements of the evolution of the perpendicular argon *ivdf* in a pulsed helicon plasma with a 1 ms time resolution using a technique very similar to that of Jackson *et al* [36].

If better time resolution is required, more sophisticated signal acquisition methods must be employed. To study the propagation of electrostatic ion shock waves in a low-density plasma by LIF, Bachet *et al* [37] used a two-channel boxcar integrator/averager. High power (>50 mW) laser light from a tuneable dye laser was mechanically chopped at 1.7 kHz, and the signal extracted from the plasma during laser ‘on’ was sent to one channel while the signal during laser ‘off’ to the other channel. Both channels’ gates were synchronized and opened for $2 \mu\text{s}$. In this way the fluorescence was discriminated from spurious emission, and the boxcar output furnished the LIF signal integrated over the gate duration. Pelissier and Sadeghi [38] and later Bachet *et al* [39] proposed another technique, which, instead of using a boxcar as a discriminator, used a multichannel scaler. Amplified with a wide band amplifier, the PMT signal was sent to a multichannel scaler having a few hundred temporal channels, each with a dwell time of $0.2 \mu\text{s}$ for the Pelissier and Sadeghi measurements and $20 \mu\text{s}$ for the Bachet *et al* measurements. During one measurement, half the channels acquire the signal corresponding to the laser ‘on’ time and the other half for the laser ‘off’ interval. The laser intensity was switched by an acousto-optic modulator synchronized with the multichannel scaler. Discrimination of the LIF light from background emission was realized by subtracting each value of the channels belonging to the second half from the corresponding number in the first half. Using this approach, measurements of electrostatic ion perturbations [40] and ion dynamics in nonlinear structures [41] were obtained with high time resolution.

For a Maxwellian distribution of particle velocities, the bulk flow velocity is obtained from the Doppler shift in the fluorescence spectrum:

$$\nu = \nu_0(1 - \mathbf{v} \cdot \mathbf{k}_L/c), \quad (1)$$

where ν is the Doppler-shifted absorption frequency, ν_0 is the rest frame absorption frequency, $\mathbf{v} \cdot \mathbf{k}_L$ is the particle velocity along the laser propagation direction \mathbf{k}_L and c is the speed of light. If Doppler broadening dominates over other line-broadening mechanisms, the temperature of the particle ensemble is inferred from the full width at half-maximum

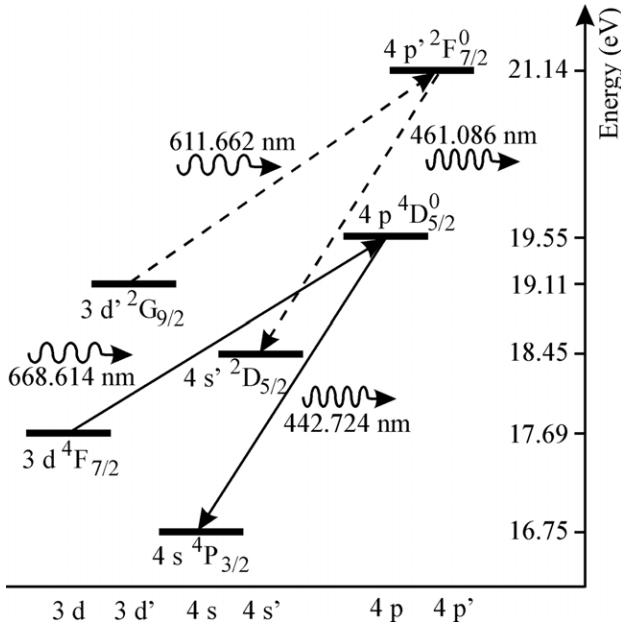


Figure 1. Partial Grotrian diagram showing the two three-level Ar II LIF schemes used in this study: $3d' \ ^2G_{9/2} \rightarrow 4p' \ ^2F_{7/2}^0 \rightarrow 4s' \ ^2D_{5/2}$ (---), accessible by dye laser and $3d \ ^4F_{7/2} \rightarrow 4p \ ^4D_{5/2}^0 \rightarrow 4s \ ^4P_{3/2}$ (—), accessible by diode laser.

($\Delta v_{1/2}$) of the fluorescence line:

$$k_B T = \left(\frac{mc^2}{8 \ln 2} \right) \left(\frac{\Delta v_{1/2}}{v_0} \right)^2, \quad (2)$$

where k_B is the Boltzmann constant, T is the particle ensemble temperature and m is the particle mass.

For parallel argon ion LIF in HELIX, we used an LIF scheme (represented by dashed lines in figure 1) in which the Ar II $3d' \ ^2G_{9/2}$ metastable state is optically pumped by 611.66 nm (vacuum wavelength) laser light to the $4p' \ ^2F_{7/2}^0$ state. The $4p' \ ^2F_{7/2}^0$ state decays to the $4s' \ ^2D_{5/2}$ state by the emission of 461.09 nm photons. The laser is a single-mode tuneable ring dye laser (Coherent 899, rhodamine 6G dye) pumped by a 6 W argon-ion laser (Coherent Innova 300) which yields about 200 mW of output power. A schematic of the LIF system used for parallel ivdf measurements in pulsed helicon plasma is shown in figure 2. After passing through a 10% beam splitter, the laser beam is modulated with a mechanical chopper at 4 kHz and then coupled in a multimode, non-polarization preserving, fibre optic cable. The fibre optic cable transports the laser light from the laser laboratory into the helicon source laboratory where several sets of laser injection and light collection optics are mounted on the HELIX and LEIA chambers. For parallel injection of laser light (to measure the parallel ivdf), a 2.54 cm collimating lens, a Galilean telescope for beam waist reducing, followed by a linear polarizer–quarter wave plate combination (Oriol™) for the conversion of the unpolarized laser light exiting the fibre optic cable into circularly polarized light are used. The collimated injection beam has a diameter of 5 mm and a power of about 40% of the power exiting the fibre optic cable. With the laser light of a single circular polarization injected along the source axis, only one of the two σ transitions, specifically

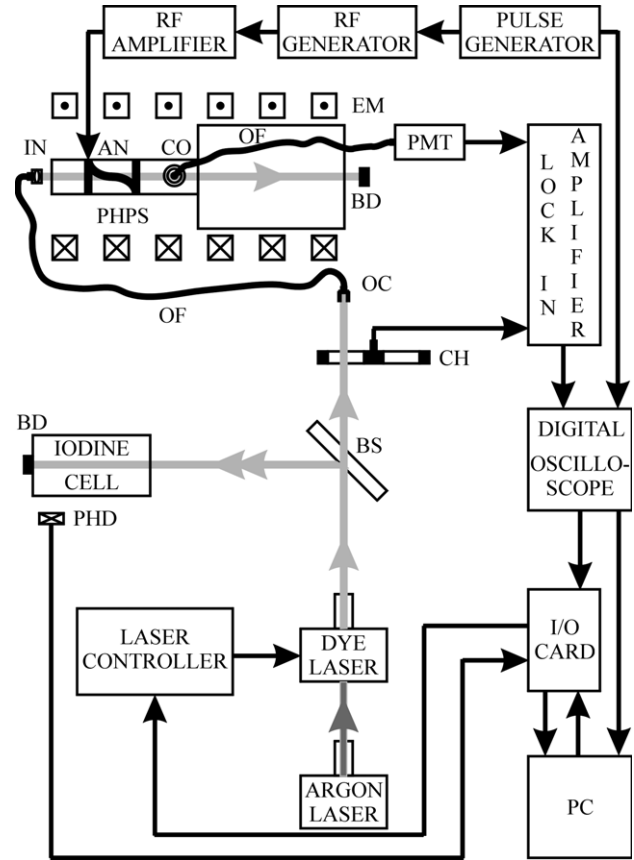


Figure 2. Experimental set-up for time resolved LIF diagnostic: PHPS—pulsed helicon plasma source, IN—injection optics, AN—antenna, CO—collection optics, BD—beam dump, EM—electromagnets, PMT—photomultiplier tube, OF—optical fibre, OC—optical coupler, CH—mechanical chopper, PHD—photo diode and BS—beam splitter.

the $\Delta M_J = +1$ transition, is optically pumped. The much smaller internal Zeeman splitting of the different $\Delta M_J = +1$ σ lines is ignored during analysis of the parallel LIF data for magnetic field strengths less than 1000 G. The 10% portion of the laser beam is passed through an iodine cell for a consistent zero velocity reference measurement to compensate for laser drift. Spontaneous emission from the iodine cell absorption lines is recorded with a photodiode for each scan of the dye laser wavelength. The fluorescence radiation is collected at 90° with respect to the laser beam by a collection optics assembly consisting of a collection lens, 10 cm focal length, 2.54 cm diameter, followed by a focusing lens, 5 cm focal length, 5 cm diameter and a multimode optical fibre cable. The numerical aperture of the focusing lens was chosen to match the numerical aperture ($NA = 0.22$) of a $200 \mu\text{m}$ -diameter fused silica optical fibre. The overlapping 5 mm diameter laser beam and 0.8 mm diameter collection focus spot yield a measurement volume of $\approx 4 \text{ mm}^3$. To increase the collected LIF signal at the expense of increased background light and poorer spatial resolution (collection focus spot of $\approx 20 \text{ mm}^2$), a 1 mm diameter optical fibre was also used for some of the measurements reported here. Light exiting the collection fibre passes through a Dell Optics 1 nm band pass interference filter centred at 461 nm. Following the filter is a Hamamatsu HC124-60 PMT detector with an integrated 20 kHz bandwidth pre-amplifier. The PMT signal

is composed of fluorescence radiation, electron impact induced radiation and electronic noise. A Stanford Research SR 830 lock-in amplifier, referenced to the modulation signal from the mechanical chopper, is used to isolate the LIF signal from background emission at the fluorescence wavelength. Lock-in amplification is indispensable since the electron-impact induced emission is several orders of magnitude larger than the fluorescence signal. The signal from the lock-in amplifier is sent to one channel of a Tektronix TDS 460A digital oscilloscope. Another channel records the pulsed waveform from the function generator used to drive the pulsed helicon discharge. The parallel drift velocity of the ions along the laser path is determined from the shift of the LIF peak relative to the iodine signal after correcting for the Zeeman shift of the σ absorption line as the laser is swept over 15 GHz. The experimental uncertainty in the ion flow speed is less than 50 m s^{-1} . Since Doppler broadening dominates the width of the measured ivdf, the parallel ion temperature is obtained from the FWHM of the distribution according to equation (2). The minimum resolvable ion temperature is 0.01 eV.

For the BWX experiments, we used a tuneable diode laser. The 8 GHz mode hop free range of the diode laser is large enough to span the absorption linewidth for 0.5 eV Ar ions. With the diode laser we used a three level argon LIF scheme (represented by full lines in figure 1) first proposed by Severn *et al* [42]. This particular LIF sequence is accessible with inexpensive tuneable diode lasers and provides good signal-to-noise ratio for a wide range of plasma conditions [43]. In this LIF scheme, the $3d^4F_{7/2}$ Ar II metastable level is optically pumped to the $4p^4D_{5/2}^0$ level by a diode laser tuned at 668.61 nm (vacuum wavelength) [44] which decays to $4s^4P_{3/2}$ by emitting fluorescence radiation at 442.72 nm. Our previous experiments have confirmed that excellent LIF signal to noise ratio for this transition sequence can be obtained with diode laser powers as small as 8 mW in steady-state argon plasmas [22, 29]. The tuneable diode laser is a Sacher Lasertechnik model Lynx-TEC100 with an external Littrow cavity comprising a piezoelectric transducer (PZT) controller grating with a beam correction mirror. This Peltier cooled diode laser is characterized by a 1.5 MHz bandwidth and 17 mW power output at a current of 85 mA. The diode laser has a coarse tuning range of approximately 8 nm around the factory set central wavelength (668 ± 4) nm. The Lynx-TEC100 has also a fine-tuning range of 0.4 nm (or 300 GHz). The Sacher Lasertechnik MLD-1000 laser controller in conjunction with a National Instruments I/O card, a Burleigh WA-1500 wavemeter, and LabWindows software are used to sweep the PZT voltage and thereby scan the laser wavelength through the absorption line over 8 GHz. Although the laser power varies slightly during such extended scans, correction of the measured LIF lineshape is realized by monitoring the laser power with an Oriel laser power meter at each laser frequency and normalizing the LIF spectrum by the measured laser power. Instead of using an iodine cell with the diode laser we used the Burleigh 1500 wavemeter for real-time wavelength monitoring. During LIF measurements, the scan rate of the laser wavelength is limited by the 1 Hz update rate of the wavemeter. The laser power after the beam splitter is approximately 15 mW. After the beam splitter, the laser light is steered into the plasma, perpendicular to the magnetic field,

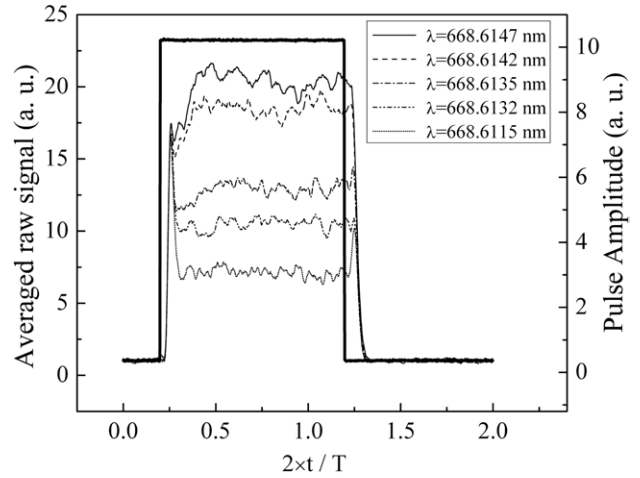


Figure 3. The rf pulse (—) and LIF signal from the lock-in amplifier for 5 distinct wavelengths averaged over 100 pulses.

with a pair of alignment mirrors. The laser polarization axis is chosen parallel to the magnetic field to avoid pumping the Zeeman split σ lines ($\Delta M_J = \pm 1$ transitions). The internal Zeeman splitting of the remaining six linearly polarized π lines ($\Delta M_J = 0$ transitions) is ignorable for the magnetic field strength of this helicon source ($< 800 \text{ G}$) [43]. The fluorescence radiation is collected at 90° with respect to the laser beam by optics mounted on a platform capable of two-dimensional motion in the plane perpendicular to the collection optics line-of-sight. The range of motion is sufficient to investigate approximately $\pm 3 \text{ cm}$ of the plasma column in the radial direction.

The LIF signal is accumulated during each plasma pulse (and dwell interval) at a digitation rate of 5 kHz and averaged over 100 cycles. After each averaged time series is acquired, the laser is tuned to a new wavelength. Typically 30 wavelengths over a laser frequency range of 8 GHz are needed to obtain reliable ion distribution function measurements. A typical rf pulse waveform is shown in figure 3. Superposed in figure 3 are time resolved LIF measurements for 5 distinct wavelengths processed by the lock-in amplifier and averaged over 100 plasma pulses. The appearance of a significant LIF signal as the laser wavelength is tuned through the absorption line is evident. After subtraction of the time-dependent background signal, the LIF signal to noise is better than 10:1. The time resolution of the measurement is limited by the integration time of the lock-in amplifier and the update rate of the lock-in output electronics. For the data shown in figure 3, the lock-in time constant was 1 ms and the lock-in output signal was updated at a rate of 512 Hz, thereby limiting the time resolution of the data in figure 3 to 1.95 ms. Close inspection of figure 3 would show the roughly 2 ms time lag in the LIF waveform relative to the plasma pulse initiation due to the 512 Hz update rate of the lock-in. Since the laser was chopped at 4 kHz, the integration time corresponds to 4 laser ‘on/off’ cycles. When set to a shorter integration time, the lock-in was unable to differentiate between the spontaneous and induced emission in the plasma. Replacing the mechanical chopper with an acousto-optic modulator operating at higher frequencies than 4 kHz would allow the time resolution to be improved while maintaining the simplicity of the lock-in

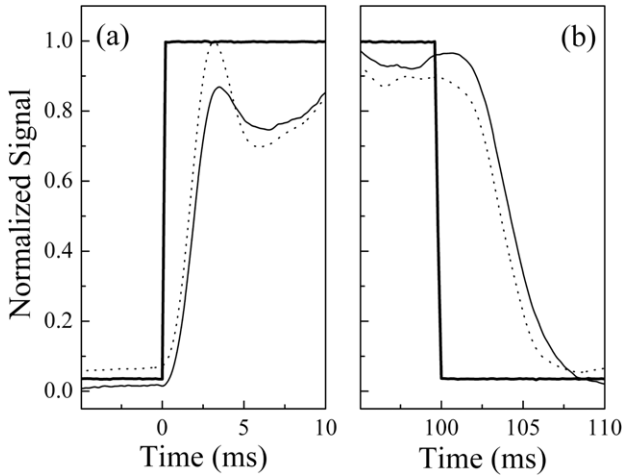


Figure 4. Expanded view of the beginning (a) and end (b) of the rf pulse amplitude (square solid line), the LIF signal from the lock-in amplifier with a 1 ms integration time (—) and the deconvoluted LIF signal (· · · · ·).

amplifier based detection scheme. By treating the lock-in integration process as a linear RC low-pass filter, improved time resolution is obtainable by digital signal processing.

Shown in figure 4 is an expanded view of the rising and falling edges of a time resolved LIF measurement for a lock-in integration time of 1 ms. Since the pulse rise time is 3 μ s for our pulse generator–rf amplifier combination, the roughly 3 ms delay rise time results from lock-in electronics. Assuming that the lock-in output voltage, $u(t)$, can be described by the convolution [36, 45].

$$u(t) = l(t) \otimes s(t), \quad (3)$$

where $s(t)$ is the signal voltage from the PMT and $l(t)$ is the low pass filter response described by

$$l(t) = \left(\frac{1}{RC} \right) H(t) \exp\left(-\frac{t}{RC}\right), \quad (4)$$

where RC is the time constant of the low pass filter and $H(t)$ is the heavy side step function. Both the left and right sides of equation (3) can be Fourier transformed to obtain

$$U(\omega) = L(\omega)S(\omega). \quad (5)$$

In practice, the measured lock-in signal and the low pass filter response are fast Fourier transformed, and then the quotient ($U(\omega)/L(\omega)$) is inverse Fourier transformed to obtain the deconvoluted PMT signal $s(t)$. The dashed curve in figure 4 is the deconvolution of the measured lock-in signal. The sharpening of the leading edge and more rapid decay of the post-pulse emission are evident in the deconvoluted data. Note that there is distinct plasma afterglow that lasts for a few milliseconds after the rf pulse ends. Nine of the thirty-one time and velocity resolved LIF measurements corresponding to those shown in figure 3 are plotted in figure 5 so that both the time and wavelength dependence of the signals are discernible. Ion velocity distributions at different times during the pulse are obtained by taking temporal slices in the LIF intensity–wavelength plane.

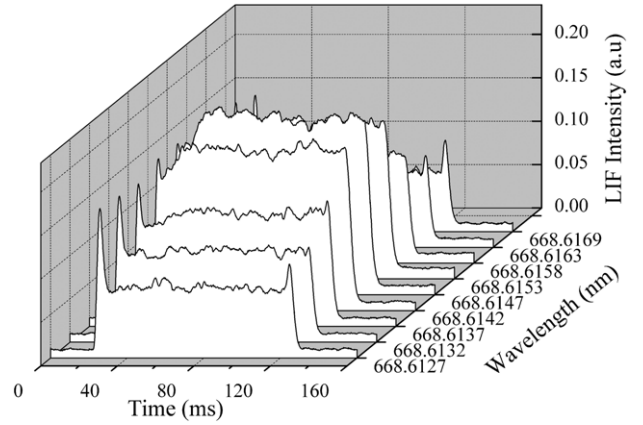


Figure 5. A set of 9 LIF signals from the lock-in amplifier averaged over 100 rf pulses without deconvolution. The data are separated by wavelength to highlight the difference in LIF signal as the laser is tuned through the absorption line.

4. Temporal evolution of parallel and perpendicular ivdfs

Recent numerical modelling has predicted [46], and experimental retarding field energy analyser [50] and LIF investigations [15] demonstrated, that in a steady-state helicon generated expanding argon plasma, near the junction between the helicon source and the diffusion chamber, two ion populations coexist: a slow moving group and a fast moving group (see figure 21 from [46], figure 10 from [50] and figure 2 from [15]). The first group is the background population, which flows at moderate velocities downstream towards diffusion chamber. The second group arises due to the formation in the expansion region, at pressures below a threshold value (typically 1–2 mTorr) of a current free EDL. The length of space charge separation, i.e. the EDL thickness is from a few tens to a few hundred Debye lengths, λ_D ($\lambda_D = \sqrt{\epsilon_0 k_B T_e / e^2 n_e}$, where ϵ_0 is the permittivity of the vacuum, k_B is the Boltzmann constant, T_e is the electron temperature, e is the elementary charge and n_e is the electron density). Depending on the EDL strength ($e\Phi / k_B T_e$, Φ —the space charge induced potential drop) the ions that pass downstream through the EDL are accelerated to velocities above the ion sound speed c_s ($c_s = \sqrt{\gamma k_B T_e / m_i}$, where m_i stands for ion mass and γ is assumed 1 for isothermal expansion). The simulations suggest that the EDL formation is triggered by the rapid decrease in electron density that occurs because of the strongly divergent magnetic field. Consistent with this explanation of EDL formation, a recent experiment by Plihon *et al* [47] demonstrated EDL formation in an axially uniform plasma with a uniform magnetic field by puffing SF₆ gas into the plasma at a single axial location. The SF₆ gas, which is highly electronegative, induces a strong electron density gradient along the plasma axis by substantially reducing the electron density, thereby simulating rapid plasma expansion without a divergent magnetic field. We note that Hatakeyama *et al* [48] demonstrated EDL formation due to a magnetic field gradient in a current driven Q-machine plasma and Kaepelin *et al* [49] also observed two ion populations in the diffusion region of a helicon discharge.

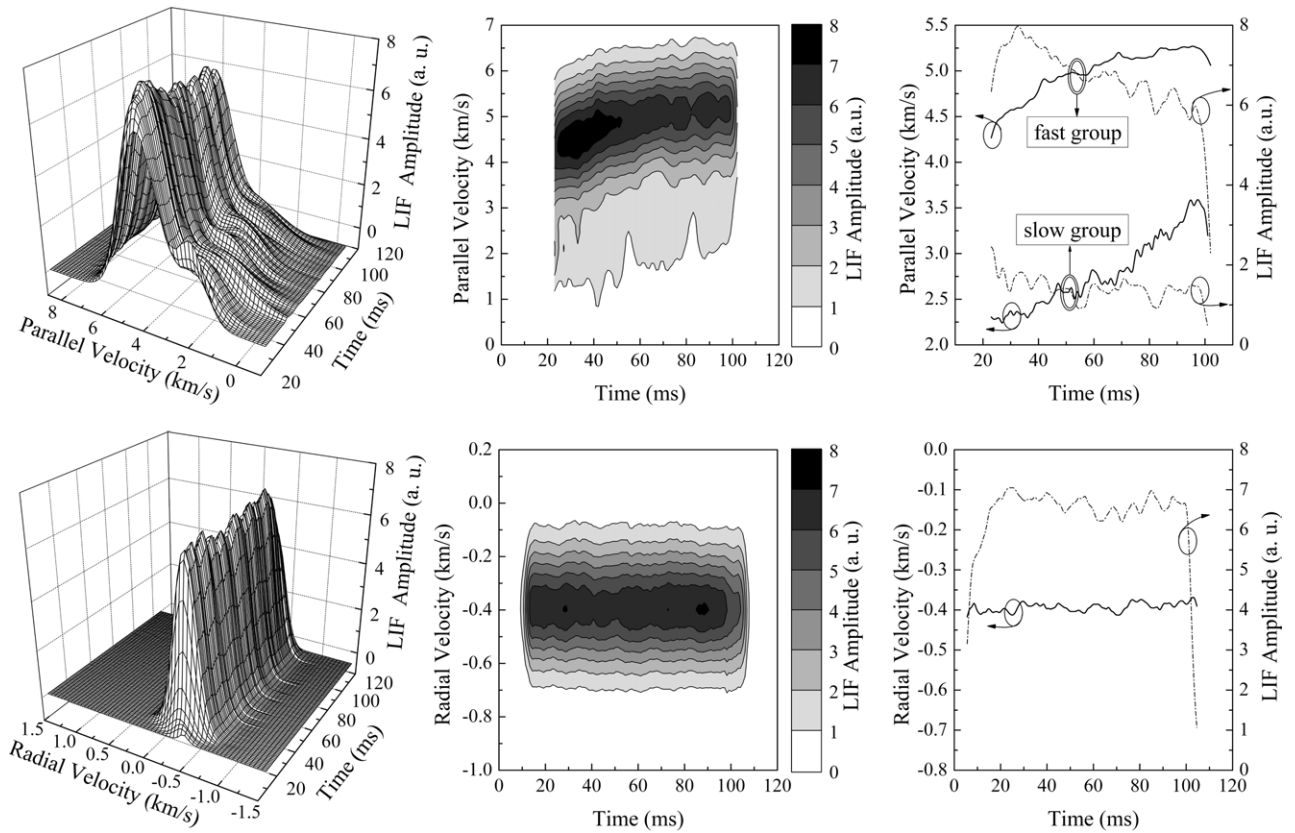


Figure 6. Temporal evolution of ivdf. Top row—parallel ivdfs in HELIX—LEIA machine; Bottom row—perpendicular ivdfs in BMW machine. Left—3D map surface plot; middle—contour plot in (v, t) plane; right—peak ion flow velocity (—) and LIF signal amplitude (— · —).

The evolution of the parallel ivdf during the rf pulse in HELIX—LEIA is shown in figure 6 for a 50% duty cycle, 5 Hz pulsed discharge. The laser was stepped through 51 wavelengths around the absorption wavelength and averaged over 100 pulses. The pressure was 0.9 mTorr, magnetic field 750 G in HELIX and zero in LEIA, rf driving frequency 9.5 MHz and the input power 800 W. As a first step, the ivdf measurements in the pulsed plasma were compared with corresponding LIF measurements in steady-state plasma. To have similar operational plasma parameters, the pressure, magnetic field strength, input power and rf driving frequency were held constant. Furthermore, once the rf matching network was tuned for steady-state operation and the ivdf measurements obtained, the discharge was switched to pulsed mode without changing the settings of the matching network or the amplitude of the rf source. Under these conditions and for long pulse ‘on/off’ intervals (100 ms), we expected that the ivdf would evolve during the pulse to a final state similar to the ivdf measurements in steady-state. Previous probe and LIF measurements in a variety of helicon sources indicate that the EDL forms on the helicon source side of the helicon source—diffusion chamber junction, where the gradient of the magnetic field is maximum. Depending on operational parameters, in HELIX-LEIA, the EDL was observed 0–20 cm upstream of the junction [15]. In Chi-Kung [50] the EDL was observed 5 cm upstream the junction. The LIF sample volume was therefore in the EDL in HELIX (4 cm inside the helicon source). Due to large random fluctuations in the emission signal during the

first 20 ms of the discharge, most likely associated with bursts of ion production during breakdown [51, 52] that saturate the lock-in amplifier, the exact moment of the formation of the fast group of ions cannot be determined from these measurements. However, two ion groups are clearly visible in the 3D graph once the signal to noise of the LIF data improves: the fast group with flow speeds between 4.2 and 5.2 km s⁻¹ and the slow group with speeds of 2.2–3.4 km s⁻¹. That the first group is created by the drift from a region of higher potential of the EDL and the slow group represents ions produced by local ionization and/or thermalization of the fast ions by charge exchange and elastic collisions can be seen by comparing the respective flow speeds to the ion sound speed. For an electron temperature of $T_e = 9$ eV, as measured with rf compensated Langmuir probe ($c_s = 4.6$ km s⁻¹) and therefore the fast ions are flowing along the magnetic field at a speed of 0.9–1.1 Mach. The slow group is flowing subsonically at 0.5–0.7 Mach. The ion temperature inferred from FWHMs of the two population distributions (see figure 7) is another indication that the fast group is formed by passing through the EDL while the slow group is generated locally. The fast ion group has a beamlike distribution function with a small energy spread ($T_{if} \approx 0.18$ eV), constant during the pulse, while the slow group ion temperature reaches $T_{is} \approx 0.5$ eV at the end of the pulse, consistent with ion heating due to charge exchange and elastic collisions [53]. As the discharge evolves, both flow speeds continue to increase. Two possible explanations are either that the EDL is moving past the measurement location or that the EDL is not fully

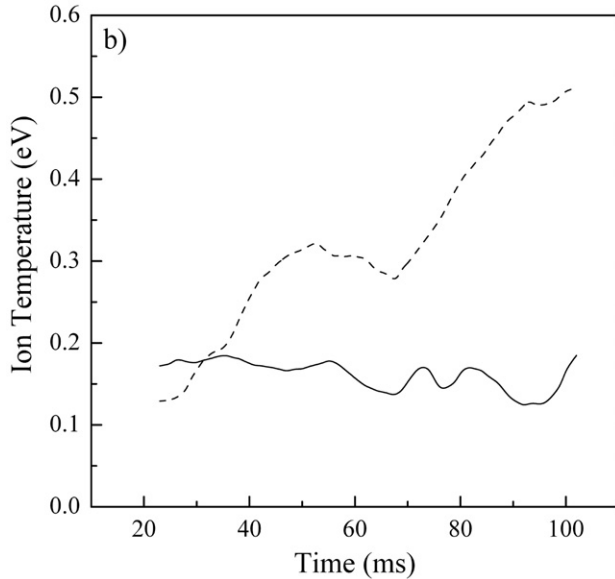
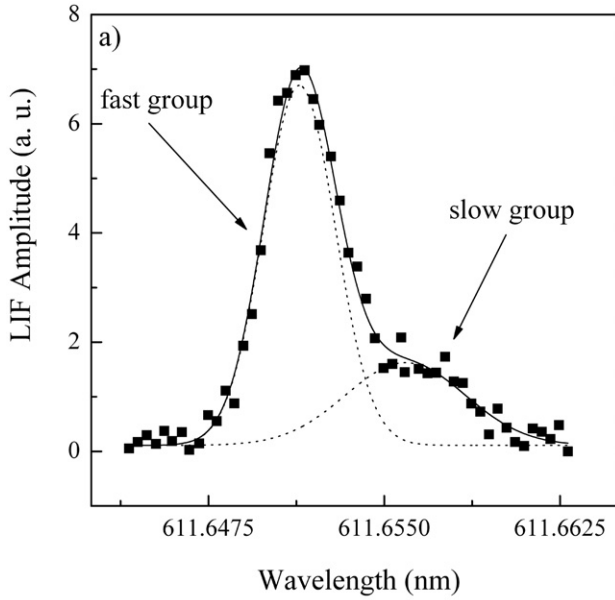


Figure 7. (a) Parallel ivdf in HELIX-LEIA machine at the moment $t = 50$ ms. Scatter graph—experimental points; —: the envelope obtained by fit with two Gaussian functions;: fit of individual Gaussian distributions. (b) The ion temperature versus time during the pulse obtained from FWHM of each ion group distribution: —: fast ion group; - - -: slow ion group.

developed and does not reach steady-state during the 100 ms pulse ‘on’ interval. The first possibility is unlikely due to the following. (a) A moving EDL similar to those observed in collisionless expanding plasmas [54] would propagate with the ion acoustic velocity, yielding a transit time across our system on the order of $\approx 300 \mu\text{s}$ —more than two orders of magnitude shorter than the rf pulse. Such short time scale phenomena are undetectable with the time resolution achieved in these experiments. However, since those experiments demonstrated that the EDL stagnates after 200–300 μs [55,56], these observations of continued evolution of the flow speed during the 100 ms pulse are inconsistent with a moving, collisionless EDL. (b) The LIF amplitude (proportional with

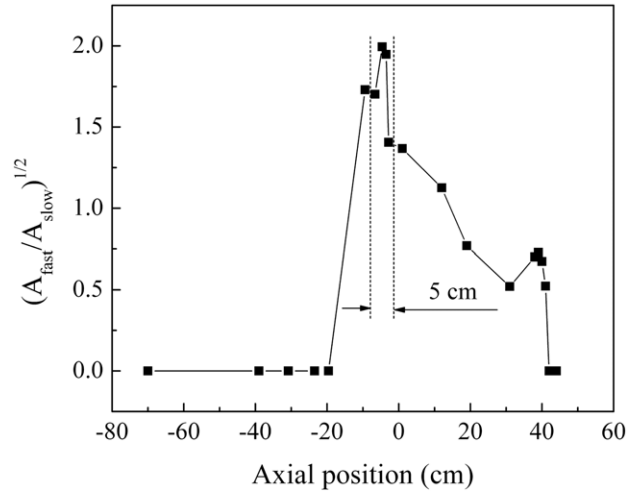


Figure 8. Axial dependence of the square root of the LIF amplitude (proportional with ion density) ratio of the fast ion group to the slow ion group. The HELIX-LEIA function is located at 0. Dotted lines mark the region in which maximum ion acceleration occurs.

the square of ion density) [14] of the slow ion population is constant during the pulse—implying a constant ionization rate at the observation location—inconsistent with a moving EDL since quasineutrality requires a larger ion density on the high potential of a EDL and therefore the ion density would increase in time. (c) For Ar^+ energies between 1.5 eV (slow group) and 5.6 eV (fast group), the total momentum transfer cross-section for Ar^+ -Ar collisions including charge exchange and elastic collisions is about $\sigma = 1.5 \times 10^{-14} \text{ cm}^2$. This cross-section yields an ion mean free path λ_{mfp} of about 4.5 cm. Additional parallel ivdf measurements were performed as a function of axial location at fixed plasmas parameters of 1.3 mTorr, 800 W and for the same magnetic configuration (see figure 8). The fast ion group was rapidly attenuated over a distance of about eight mean free paths, i.e. the square root of amplitude of the fast ion population LIF signal normalized to the slow ion population decreased from 2 in the EDL to about 0.5 at 35 cm downstream of the EDL. Therefore, if an EDL was moving past the LIF measurement location either a decrease or an increase in the ratio of fast to slow population LIF amplitude would be observed. Since the square root of LIF amplitude ratio is nearly constant ≈ 2.2 throughout the time resolved measurement interval, a moving EDL is unlikely to be responsible for the observed evolution in the flow speeds.

The second possibility, that the EDL is not yet fully formed after 100 ms, is more likely given that in steady-state operation the speed of the fast ion group is about 7.8 km s^{-1} (1.7 Mach), much higher than the flow speed observed at the end of the 100 ms pulse. Such high ion speeds correspond to a potential drop across the EDL of $\Phi \approx 13 \text{ V}$, more than double than what is observed at the end of the pulse. On the low speed side of the slow group portion of the ivdf, the distribution has a long, non-Maxwellian tail—consistent with the creation of the slow ion group in the EDL and subsequent acceleration by a fraction of the total potential across the EDL. Note also that the nearly identical rates of speed increase, $\approx 14 \text{ m s}^{-2}$, for both the slow and fast ion groups during the pulse is consistent with an increasing potential drop across the EDL.

Applying the electron flux balance equation to the boundary of two different plasmas and assuming that the generated thermoelectric field vanishes at the foot of the EDL, Chan *et al* [57] found that the strength of the EDL that forms between two plasmas obeys

$$\exp(-e\Phi/k_B T_{eH}) = n_{eL} T_{eL}^{3/2} / n_{eH} T_{eH}^{3/2}, \quad (6)$$

where the subscripts H and L correspond to the high and low potential sides of the EDL, respectively. Based on their model, a qualitative picture of EDL temporal evolution can be formulated as follows. Once the EDL forms, the flow of ions and electrons upstream and downstream, respectively, is limited. The positive and negative space charge on the high potential side and the low potential side of the EDL will build up and the EDL strength will increase until equilibrium is reached, i.e. when the number of energetic electrons from the tail of the electron distribution function on the high potential side able to overcome the potential barrier balances the number of electrons crossing the EDL from the low potential side. Therefore, downstream of the EDL we observe that the speed of the fast ion population (ions accelerated through upstream presheath and EDL) increases during the pulse since the space charge and consequently the potential drop across the EDL is increasing. Since our observation point is in the EDL, the slow ion population can be associated with the local ionization process in the strengthening EDL and is accelerated by only a portion of the total potential drop across the EDL (the slow ions resulted from charge-exchange process should be insignificant since the mean free path for this process is longer than the EDL thickness). For our plasma parameters, $T_{eH} = 9 \text{ eV}$, $n_{eH} = 2 \times 10^{11} \text{ cm}^{-3}$ in HELIX and $T_{eL} = 6 \text{ eV}$, $n_{eL} = 5 \times 10^{10} \text{ cm}^{-3}$ in LEIA [14], equation (6) predicts a steady-state potential drop of $\approx 18 \text{ V}$, which is in reasonable agreement with the $\approx 13 \text{ V}$ potential drop estimated from the flow velocity data.

In a recent probe-based study of the time evolution of an EDL in a helicon source, Charles and Boswell [32] found that the EDL forms within $\approx 100 \mu\text{s}$ of the beginning of the pulse. In spite of significant structural differences between the Chi-Kung and HELIX helicon sources (Chi-Kung has insulated Pyrex wall at the source–expansion chamber while HELIX has a grounded metal wall) which may give rise to different potential profiles (the source wall should charge up to allow the potential drop to occur in the plasma in Chi-Kung, while in HELIX currents can close through the walls), the EDL in Chi-Kung was also found to require 100–200 ms to reach a steady-state [58].

Shown in the second row of figure 6 is the evolution of the perpendicular ivdf in the BWX machine for the same pulse length and duty cycle as for the parallel measurements. The perpendicular ivdf evolution was obtained by stepping the laser over 31 wavelengths around the absorption wavelength 668.6138 nm and averaging over 100 pulses. The collection optics was 20 cm downstream of the aluminium plate at the source/chamber junction and viewed plasma 2 cm from the source axis. The pressure was 1 mTorr, magnetic field 260 G and rf driving frequency 13.56 MHz. Since the lower rf power of 300 W yielded a quieter discharge breakdown phase, a good LIF signal was obtained after the first 4 ms of the pulse. The shift in frequency of the peak LIF emission frequency was

relatively constant throughout the discharge. The inferred values of the bulk ion speed show a modest outward ion flow (radially outward) of about 400 m s^{-1} and no evidence of ion acceleration and electric field structures in radial direction. The perpendicular ion temperature calculated from Gaussian fits to the measured ivdf is a nearly constant 0.05 eV, yielding an ion thermal speed of 400 m s^{-1} —comparable to the measured bulk radial diffusion speed. The LIF measurements obtained during the plasma afterglow indicate that the rate of decrease of the perpendicular ion temperature is much smaller than the rate of decrease in the LIF intensity. Thus, it is possible that afterglow measurements could be used to investigate both the energy and plasma confinement times of helicon source plasmas [59]. Assuming that in the afterglow creation of the $3d^4F_{7/2}$ argon ion metastable state (Ar^{**}) by electron collisions ceases (the formation of the metastable state requires 33.4 eV for direct ionization and excitation of the ground state neutral Ar or for stepwise ionization, 15.7 eV for ionization and 17.7 eV for excitation) and neglecting other channels of $3d^4F_{7/2}$ formation ($e\text{-Ar}^{2+}$ recombination, Ar_2^+ conversion, collisions and cascading from upper levels), and only considering loss of the ions in this state by radial ambipolar diffusion and quenching by electrons, the rate equation for $3d^4F_{7/2}$ ions may be written as

$$\frac{\partial n_i^*(t)}{\partial t} = D_a(t) \nabla^2 n_i^*(t) - k_{eq} n_e(t) n_i^*(t), \quad (7)$$

where $n_i^*(t)$ is the Ar^{**} density, $n_e(t)$ is the electron density and k_{eq} is the quenching rate (including recombination) of this state by collisions with electrons. Since, in the early afterglow, there is a rapid decrease in electron temperature and density [60,61], exponential decay $\exp(-t/\tau_e)$ of the electron density $n_e(t)$ and the ambipolar diffusion coefficient $D_a(t)$ is also assumed. The initial state is set at the beginning of the afterglow and τ_e is the electron density characteristic decay time (on the order of $300 \mu\text{s}$ [7,62]). By replacing the spatially dependent diffusion term by the lowest order spatial mode (assuming that the 0 mode goes to zero at the chamber walls), equation (7) may be written as

$$\frac{\partial n_i^*(t)}{\partial t} = - \left[\frac{D_a(0)}{\Lambda^2} + k_{eq} n_e(0) \right] \exp\left(-\frac{t}{\tau_e}\right) n_i^*(t), \quad (8)$$

where Λ is the length of the lowest order mode $1/\Lambda^2 = (2.4/R)^2 + (\pi/L)^2$ (R and L are the radius and the length of the diffusion chamber, respectively). For magnetized plasmas the transverse ambipolar diffusion coefficient D_a may be written as [63]

$$D_a(0) \approx \frac{D_i T_e / T_i}{1 + \mu_e \mu_i B^2}, \quad (9)$$

where D , T , μ and B are the diffusion coefficient, temperature, mobility and magnetic field strength with indexes i and e for ions and electrons, respectively. From radial flow data we infer a value of the reduced electric field of $E/n \approx 47 \text{ Td}$ ($1 \text{ Td} = 10^{-17} \text{ V cm}^2$) which then gives $\mu_i \approx 1230 \text{ cm}^2 (\text{V s})^{-1}$ and $\mu_e = 3 \times 10^5 \text{ cm}^2 (\text{V s})^{-1}$ [64,65]. For our plasma conditions ($T_e = 3 \text{ eV}$, $T_i = 0.05 \text{ eV}$, $B = 260 \text{ G}$) and with values of the free ion diffusion of $D_i = 35 \text{ cm}^2 \text{ s}^{-1}$ [66], $D_a(0) \approx 2100 \text{ cm}^2 \text{ s}^{-1}$ at the end of the pulse, which is in good agreement with the estimated value for an electron beam generated argon plasma with 150 G axial magnetic field and

$T_e = 1 \text{ eV}$ [67]. Although ambipolar diffusion is a relatively slow process compared with quenching by electrons, for these particular conditions the diffusion time scale (Λ^2/D_a) at the end of the pulse is on the order of a few milliseconds. Equation (8) can be solved analytically:

$$n_i^*(t) = n_i^*(0) \exp \left\{ -\tau_e \left[k_{\text{eq}} n_e(0) + \frac{D_a(0)}{\Lambda^2} \right] \right. \\ \left. \times \left[1 - \exp \left(-\frac{t}{\tau_e} \right) \right] \right\} \quad (10)$$

and the quenching rate is given by

$$k_{\text{eq}} = \frac{1}{n_e(0)} \left[\frac{1}{\tau_e [1 - \exp(-\tau_i/\tau_e)]} - \frac{D_a(0)}{\Lambda^2} \right], \quad (11)$$

where τ_i is the metastable ion density characteristic decay time. Thus, a simple exponential fit to the square root of the LIF signal in the afterglow yields a $1/e$ time of 1.2 ms, equivalently an electron quenching rate of $k_{\text{eq}} \approx 3.33 \times 10^{-10} \text{ cm}^3 \text{ s}^{-1}$. This value is roughly a factor of 6 smaller than the total quenching rate inferred from effective quenching cross-section of Ar^{+*} ($3d^4F_{7/2}$) metastable state estimated by Cohen *et al* ($\sigma = 5.15 \times 10^{-14} \text{ cm}^2$) [12]. Based on the flow speed ($V = 400 \text{ m s}^{-1}$ from LIF measurements), $K_q \approx \sigma \times V \approx 2.1 \times 10^{-9} \text{ cm}^3 \text{ s}^{-1}$. This discrepancy may come from the simplifying assumptions used here (the quenching by collisions with Ar neutral atoms may be significant) and/or, most probably, from the overestimation of the metastable ion density decay time introduced by the RC time constant of this lock-in integration based detection method.

5. Discussion

In summary, by using a LIF diagnostic technique with a time resolution of 1 ms, we have investigated the temporal evolution of the ivdf in two different pulsed helicon discharges. The parallel ivdf measurements confirm that in the expansion region of a helicon generated plasma, for certain operational conditions, two ion populations exist: a fast ion group having a beamlike distribution, accelerated to supersonic speed by an EDL, and a slow moving group formed by local ionization. Analysis of the ivdf temporal evolution shows that in a collisional plasma, although it forms within 20 ms, the double layer has not reached a steady-state by 100 ms into the rf pulse. This is in contrast to EDLs created by plasma expansion into a vacuum where steady-state EDLs were observed after only a few hundred microseconds. In a qualitatively similar helicon source, although the EDL appeared in about 100 μs , a steady-state EDL also required 100–200 ms. Measurements of perpendicular ivdf evolution in a pulsed plasma show little change throughout the pulse. Modest and steady radially outward flows on the order of the ion thermal speed were observed.

For plasma thruster concepts with magnetic nozzles, using a pulsed operation instead of steady-state may resolve the contradicting requirements of efficient plasma acceleration and plasma detachment. Since detachment of the plasma flow from the vacuum magnetic field lines can occur only after the kinetic energy density of the plasma flow exceeds the energy density of the diverging magnetic field of the nozzle, pulses with

pulse ‘on’ times just long enough to fulfil the above condition might be an efficient means of generating high energy density plasmas that then detach.

For plasma enhanced chemical vapour deposition, pulsed discharges provide additional control of the deposition process and the quality of the deposited films. Control of the directed ion energy during the pulse ‘on’ time and subsequent ion distribution relaxation during the pulse ‘off’ time may allow *in situ* switching between different deposition process characteristics (ion energy, ion flux density, ion flux uniformity) during the film growth process.

In plasma etching, the substrate bias used to accelerate ions into the wafer results in spatially dependent charging of the wafer and a phenomenon known as electron shading [68]. Electron shading, which causes sidewall profile damage and etching yield reduction, can be significantly reduced by modulating the source power and bias voltage. However, since an energetic ion population spontaneously exits the helicon source, substrate bias is unnecessary and electron shading could be avoided altogether.

Finally, many of the pulsed discharges used in plasma processing have pulse ‘on’ times that range from 10 ms to a few hundred milliseconds. Therefore, the LIF diagnostic method described in this work is suitable for temporal investigations of ivdfs in a wide range of commercially interesting plasmas.

Acknowledgments

This work was supported by US Department of Energy EPSCoR Laboratory Partnership Program grant ER45849 and NSF grant PHY-0315356.

References

- [1] Charles C, Boswell R W and Porteous R 1992 *J. Vac. Sci. Technol. A* **10** 398
- [2] Charles C and Boswell R W 1995 *J. Vac. Sci. Technol. A* **13** 2067
- [3] Chen F, Jiang X and Evans J 2000 *J. Vac. Sci. Technol. A* **18** 2108
- [4] Chen F F, Evans J D and Tynan G R 2001 *Plasma Sources Sci. Technol.* **10** 236
- [5] Perry A and Boswell R W 1989 *Appl. Phys. Lett.* **55** 148
- [6] Charles C and Boswell R W 1998 *J. Appl. Phys.* **84** 350
- [7] Clarenbach B, Lorentz B, Kramer M and Sadeghi N 2003 *Plasma Sources Sci. Technol.* **12** 345
- [8] Glover T W, Chang Diaz F R, Squire J P, Jacobson V P, Chavers D G and Carter M D 2005 *AIP Conf. Proc.* **746** 976
- [9] Boswell R W *et al* 2004 *Phys. Plasmas* **11** 5125
- [10] Spektor R and Choueiri E Y 2004 *Phys. Rev. E* **69** 046402
- [11] Charles C and Boswell R W 2003 *Appl. Phys. Lett.* **82** 1356
- [12] Cohen S A, Siefert N S, Stange S, Scime E E, Boivin R F and Levinton F 2003 *Phys. Plasmas* **10** 2593
- [13] Charles C 2004 *Appl. Phys. Lett.* **84** 332
- [14] Sun X, Biloiu C, Hardin R and Scime E 2004 *Plasma Sources Sci. Technol.* **13** 359
- [15] Sun X, Keesee A, Biloiu C, Scime E, Meige A, Charles C and Boswell R W 2005 *Phys. Rev. Lett.* **95** 025004
- [16] Winglee R M, Ziembra T, Euripides P and Slough J 2002 *AIP Conf. Proc.* **608** 433
- [17] Ziembra T, Slough J and Winglee R M 2005 *AIP Conf. Proc.* **746** 945
- [18] Stern R A and Johnson J A III 1975 *Phys. Rev. Lett.* **34** 1548
- [19] Hill D H, Fornaca S and Wickham M G 1983 *Rev. Sci. Instrum.* **54** 309

- [20] Goecker M J and Goree J 1989 *J. Vac. Sci. Technol. A* **7** 977
- [21] Trevor D J, Sadeghi N, Nakano T and Derouard J 1990 *Appl. Phys. Lett.* **57** 1188
- [22] Keesee A M, Scime E E and Boivin R 2004 *Rev. Sci. Instrum.* **75** 4091
- [23] Zintl M and McWilliams R 1994 *Rev. Sci. Instrum.* **65** 2574
- [24] Biloiu C, Scime E, Sun X and McGeehan B 2004 *Rev. Sci. Instrum.* **75** 4296
- [25] Zimmerman D C, McWilliams R and Edrich D A 2005 *Plasma Sources Sci. Technol.* **14** 581
- [26] Amorim J, Baravian G and Jolly J 2000 *J. Phys. D: Appl. Phys.* **33** R51 (and references therein)
- [27] Foley E and Levinton F 2004 *Rev. Sci. Instrum.* **75** 3462
- [28] Noonan W, Jones T and Ottinger P 1997 *Rev. Sci. Instrum.* **68** 1032
- [29] Scime E, Biloiu C, Compton C, Doss F, Ventura D, Heard J, Choueiri E and Spektor R 2005 *Rev. Sci. Instrum.* **76** 026107
- [30] Spektor R and Choueiri E *Proc. 38th Joint Propulsion Conf. (Indianapolis, IN, 7–10 July 2002)* AIAA 2002-3801
- [31] Spektor R and Choueiri E *Proc. 40th Joint Propulsion Conf. (Ft. Lauderdale, FL, 11–14 July 2004)* AIAA 2004-4095
- [32] Charles C and Boswell R W 2004 *Phys. Plasmas* **11** 3808
- [33] Sarfaty M, De Souza-Machado S and Skiff F 1996 *Phys. Plasmas* **3** 4316
- [34] Sudit I and Chen F F 1994 *Plasma Sources Sci. Technol.* **3** 162
- [35] Scime E, Boivin R, Kline J and Balkey M 2001 *Rev. Sci. Instrum.* **72** 1672
- [36] Jackson G, Lewis C, Doorn S, Majidi V and King F 2001 *Spectrochim. Acta B* **56** 2449
- [37] Bachet G, Cherigier L, Arnas-Capeau C, Doveil F and Stern R A 1996 *J. Phys. III France* **6** 1157
- [38] Pelissier B and Sadeghi N 1996 *Rev. Sci. Instrum.* **67** 3405
- [39] Bachet G, Skiff F, Dindelegan M, Doveil F and Stern R A 1998 *Phys. Rev. Lett.* **80** 3260
- [40] Bachet G, Skiff F, Doveil F and Stern R A 2001 *Phys. Plasmas* **8** 3535
- [41] Skiff F, Bachet G and Doveil F 2001 *Phys. Plasmas* **8** 3139
- [42] Severn G D, Edrich D A and McWilliams R 1998 *Rev. Sci. Instrum.* **69** 10
- [43] Boivin R F and Scime E E 2003 *Rev. Sci. Instrum.* **74** 4352
- [44] National Institute of Standards and Technology *Atomic Spectra Database* <http://physics.nist.gov/cgi-bin/AtData/main.asd>
- [45] Jansson P A 1984 *Deconvolution: With Applications in Spectroscopy* (Orlando, FL: Academic)
- [46] Meige A, Boswell R W, Charles C and Turner M 2005 *Phys. Plasmas* **12** 052317
- [47] Plihon N, Corr C S and Chabert P 2005 *Appl. Phys. Lett.* **86** 091501
- [48] Hatakeyama R, Suzuki Y and Sato N 1983 *Phys. Rev. Lett.* **50** 1203
- [49] Kaepelin V, Carrere M and Layet J-M 2002 *J. Vac. Sci. Technol. A* **20** 526
- [50] Charles C and Boswell R W 2004 *Phys. Plasmas* **11** 1706
- [51] Boswell R W and Vender D 1995 *Plasma Sources Sci. Technol.* **4** 534
- [52] Conway G D, Perry A J and Boswell R W 1998 *Plasma Sources Sci. Technol.* **7** 737
- [53] Anderegg F, Stern R A, Skiff F, Hammel B A, Tran M Q, Paris P J and Kohler P 1986 *Phys. Rev. Lett.* **57** 329
- [54] Hairapetian G and Stenzel R 1988 *Phys. Rev. Lett.* **61** 1607
- [55] Hairapetian G and Stenzel R 1991 *Phys. Fluids B* **3** 899
- [56] Chan C, Cho M H, Hershkovitz N and Intrator T 1984 *Phys. Rev. Lett.* **52** 1782
- [57] Chan C, Hershkovitz N and Lonngren K 1983 *Phys. Fluids* **26** 1587
- [58] Charles C 2005 Private communication
- [59] Balkey M, Boivin R, Keiter P A, Kline J L and Scime E E 2001 *Plasma Sources Sci. Technol.* **10** 284
- [60] Sugawara M, Okada T and Kobayashi Y 1986 *J. Phys. D: Appl. Phys.* **19** 1213
- [61] Okada T and Sugawara M 1986 *J. Phys. D: Appl. Phys.* **26** 1680
- [62] Kaepelin V, Carrere M and Layet J M 2002 *Plasma Sources Sci. Technol.* **11** 53
- [63] Phelps A V 1990 *J. Res. Natl Inst. Stand. Technol.* **95** 407
- [64] Brown S C 1994 *Basic Data of Plasma Physics* (New York: AIP)
- [65] Mustata I and Biloiu C 1998 *Contrib. Plasma Phys.* **38** 447
- [66] Markovic V Lj, Gocic S R, Stamenkovic S N and Perovic Z Lj 2005 *Phys. Plasmas* **12** 073502
- [67] Walton S G, Leonhardt D and Fernsler R F 2005 *IEEE Trans. Plasma Sci.* **33** 838
- [68] Sumiya M, Tamura H and Watanabe S 2002 *Japan. J. Appl. Phys.* **41** 856